Journal of King Saud University (Science) (2009) **21**, 133–143

King Saud University
Journal of King Saud University (Science)
www.ksu.edu.sa
www.sciencedirect.com

ORIGINAL ARTICLE

Kinetic analysis of nonisothermal decomposition of ($Mg_5(CO_3)_4(OH)_2{\cdot}4H_2O/5Cr_2O_3$) crystalline mixture

Asma A. Al-Othman *, Khalid A. Al-Farhan, Refaat M. Mahfouz

Department of Chemistry, College of Science, King Saud University, Riyadh, Saudi Arabia

Received 25 January 2009; accepted 13 April 2009
Available online 5 August 2009

KEYWORDS

Thermal decomposition;
Model fitting;
Model free;
Isokinetic;
Kinetic parameter;
$MgCr_2O_4$ spinel

Abstract Pure $MgCr_2O_4$ spinel was synthesized from crystalline mixture of ($Mg_5(CO_3)_4(OH)_2{\cdot}4H_2O/5Cr_2O_3$) by heating at 900 °C for 27 h. TG, DTA, FT-IR and XRPD techniques were used to follow the reactions and identify the products. Nonisothermal kinetics of thermal decomposition of un-irradiated and γ-irradiated physical crystalline mixtures were studied in static air. The kinetic parameters were obtained through model-fitting and model-free methods, and artificial isokinetic relationship (IKR) for multi-step processes. The results show that the decomposition for both un-irradiated and γ-irradiated mixtures proceed through two steps with different reaction mechanisms. The first is a third-order reaction (F_3) mechanism followed by one-dimensional diffusion (D_1) as a second step.

1. Introduction

The tremendous increase in the development of the industrial and transportation sectors have led to consumption of huge quantities of fuel which results in an increase in the amount of hazardous gases such as NO_x, CH and CO_x emitted to the environment. Low cost transition metal mixed oxides such as spinels are active in catalytic total oxidation processes aimed at limiting of air pollution, which often is carried out on the more expensive noble metal-based catalysts. Spinels with AB_2O_4 formula such as pirochromite $MgCr_2O_4$ have additional important technological applications such as magnetic materials, high temperature ceramics, combustion catalysis, catalytic support, strength agents, sensor elements and inter connection materials for solid oxide fuel cells (Shimizu et al., 1990; Gengembre et al., 1999; Docherty et al., 2001). $MgCr_2O_4$ is normal spinel has space group F3dm, with 56 atoms per unit cell ($Z = 8$), Mg and Cr ions occupy the tetrahedral and octahedral site, respectively (Bhatta and Nayak, 2002).

Thermal decomposition of various compounds are of major importance because of their frequent applications in calcinations metallurgy and in the production of large-surface materials for sorbents and catalysis (Hartman et al., 1994). Many studies have been carried out on the effect of γ-irradiation on the thermal decomposition of inorganic solids (Monshi et al., 1998; Mahfouz et al., 2000, p. 59). In general, the effects with increasing dose are in changing of the induction period and acceleration of the decomposition process i.e. the decrease

* Corresponding author.
E-mail address: asmaalothman@yahoo.com (A.A. Al-Othman).

1018-3647 © 2009 King Saud University. All rights reserved. Peer-review under responsibility of King Saud University.
doi:10.1016/j.jksus.2009.04.001

Production and hosting by Elsevier

in time or temperature required to complete the reaction in case of the pre-irradiated material which were attributed to formation of additional nucleation site and reactive center (Mahfouz et al., 2000, p. 363).

In the present work, we report the kinetic studies of the thermal decomposition of crystalline mixtures ($Mg_5(CO_3)_4(OH)_2{\cdot}4H_2O/5Cr_2O_3$) before and after γ-irradiation by applying model-fitting and model-free kinetic approaches to the nonisothermal thermoanalytical data. Formation of magnesium chromite from above materials is also reported. TG, DTA, FT-IR and XRPD techniques were used to follow the reactions and identify the products.

2. Experimental

Powder of heavy magnesium carbonate hydrate $Mg_5(CO_3)_4(OH)_2{\cdot}4H_2O$ and Cr_2O_3 were obtained commercially from (BDH reagent grade) and were used without any further purifications. 1:5 molar ratio mixtures of the starting materials were calcined at different temperature in the range (100–900 °C) for 9 h each. For irradiation, samples were encapsulated under vacuum in glass vials and were exposed to successively increasing doses of γ-irradiation at constant intensity using Co-60 γ-ray cell 220 (Nordion MDS, Ontario, Canada) at a dose rate of 10^2 kGy/h. The source was calibrated against Fricke ferrous sulfate dosimeter, and the dose rate in the irradiated samples was calculated by applying appropriate corrections on the basis of photon mass attenuation and energy-absorption coefficient for the sample and the dosimeter solution (Spinks and Woods, 1990). IR spectra were recorded as KBr pellets using a Perkin–Elmer 1000 FT-IR spectrometer. XRPD measurements were carried out on a Jeol D8030 X-ray diffractometer using a nickel filter (Cu Kα $\lambda = 1.5418$ Å). The thermal decomposition of physical mixture was followed by nonisothermal (dynamic) thermogravimetric techniques using TGA-7 (Perkin–Elmer) thermogravimetric analyzer. Dynamic experiments were performed at heating rate 5, 10, 15, 20 and 25 °C/min.

3. Result and discussion

3.1. X-ray powder diffraction (XRPD) analysis

Fig. 1 shows XRPD patterns of the calcined mixtures at different temperatures for different duration times. All phases in the mixtures were identified by FARHAN program (Al-Farhan, 1999). The XRPD pattern of the mixture heated at 300 °C displays only the peaks of Cr_2O_3, indicating that the heavy magnesium carbonate hydrate had converted to amorphous lower carbonate as documented by FT-IR measurement (see Fig. 2). The XRPD of the mixture calcined at 500 °C shows only the characteristic peaks of Cr_2O_3 and MgO. No notable changes in XRPD of the mixtures heated up to 600 °C were detected compared with that heated at 500 °C. The XRPD of the mixture calcined at 625 °C are dominated by the peaks of Cr_2O_3 and MgO, with the main characteristic peaks of $MgCr_2O_4$ just starting to show up in the XRPD. $MgCr_2O_4$ becomes the dominant phase in the mixture calcined at 900 °C for 9 h. $MgCr_2O_4$ is the only phase present in the XRPD pattern of the mixture heated at 900 °C for 27 h. The same result was obtained from the counterpart of irradiated mixture.

3.2. FT-IR analysis

Fig. 2 shows the FT-IR spectra of the starting materials before and after γ-irradiation. The spectrum of un-irradiated heavy magnesium carbonate hydrate (a) shows bands of the carbonate anion at 1120 cm^{-1} (symmetric stretching), 1485 and 1423 cm^{-1} (asymmetric stretching), 745 and 714 cm^{-1} (symmetric bend), and 854, 886 and 797 cm^{-1} (asymmetric bend). The two main bands at 3515 and 3450 cm^{-1} are due to lattice water vibration and the 3649 cm^{-1} is due to OH^- stretching (White, 1971). Spectrum (c) shows five main bands at 637, 569, 443, 415 and 305 cm^{-1} which are due to lattice vibration of un-irradiated Cr_2O_3. Neither disappearance nor appearance of new bands was observed as result of γ-irradiation up to 10^3 kGy total γ-ray dose as well as seen in (b and d, respectively).

The FT-IR spectra for the calcined mixtures are shown in Fig. 3. The spectra of the mixture calcined at 300 °C shows main bands at 643, 573, 442, 413 and 305 cm^{-1} which are due to Mg–O and Cr–O lattice vibrations, and the weak band at 858 cm^{-1} is due to carbonate anion. At 500 °C, the spectra displays, in addition to, lattice vibration bands of MgO and Cr_2O_3, two bands at 957 and 834 cm^{-1} which are due to Cr═O stretching of amorphous α-$MgCrO_4$ (Roy et al., 1969). At 625 °C, the bands of α-$MgCrO_4$ completely disappeared from the spectra, and the characteristic band of $MgCr_2O_4$ at 429 cm^{-1} (Willey et al., 1993) is not detectable, although it present and it was confirmed by XRPD. However, the 429 cm^{-1} band is observable in FT-IR spectra of the mixture heated at 650 °C. The spectra of the mixture calcined at 900 °C for 27 h displays only the bands of $MgCr_2O_4$, and the characteristic band of Cr_2O_3 at 305 cm^{-1} is completely disappeared.

3.3. TG and DTA analysis

Fig. 4 shows TG and DTA curves for thermal decomposition of heavy magnesium carbonate in a pure form and in physical mixture with chromium(III)oxide.

Fig. 4a shows typical TG–DTA curves of the thermal decomposition of pure heavy magnesium carbonate hydrate. The TG of pure salt showed three overlapped decomposition steps. The first decomposition step was in the range of (100–250) °C attributed to loss of water of crystallization, this decomposition was accompanied by an endothermic peak at 230 °C. The second decomposition step was in the range of (370–440) °C due to loss of hydroxyl water and was accompanied by an endothermic peak at 430 °C. The third decomposition step was in the range of (440–500) °C due to decomposition of $MgCO_3$ and was accompanied by sharp endothermic peak at 480 °C. Very sharp exothermic peak was detected at 460 °C attributed to the crystallization of $MgCO_3$ from the amorphous lower carbonate (Criado et al., 1979; Khan et al., 2001; Sawada et al., 1979a, p. 32, 1979b, p. 33, 1979c, p. 34).

Fig. 1b shows the TG and DTA curves of crystalline mixture. The DTA show an endothermic peak detected at almost the same temperature range as for pure salt for loss of water of crystallization. A more broad second endothermic peak was detectable at 440 °C due to loss of hydroxyl water and starting to form the chromate intermediate. Two endothermic peaks were detectable at 490 °C and 500 °C due to the decomposition of chromate intermediate and formation of amorphous

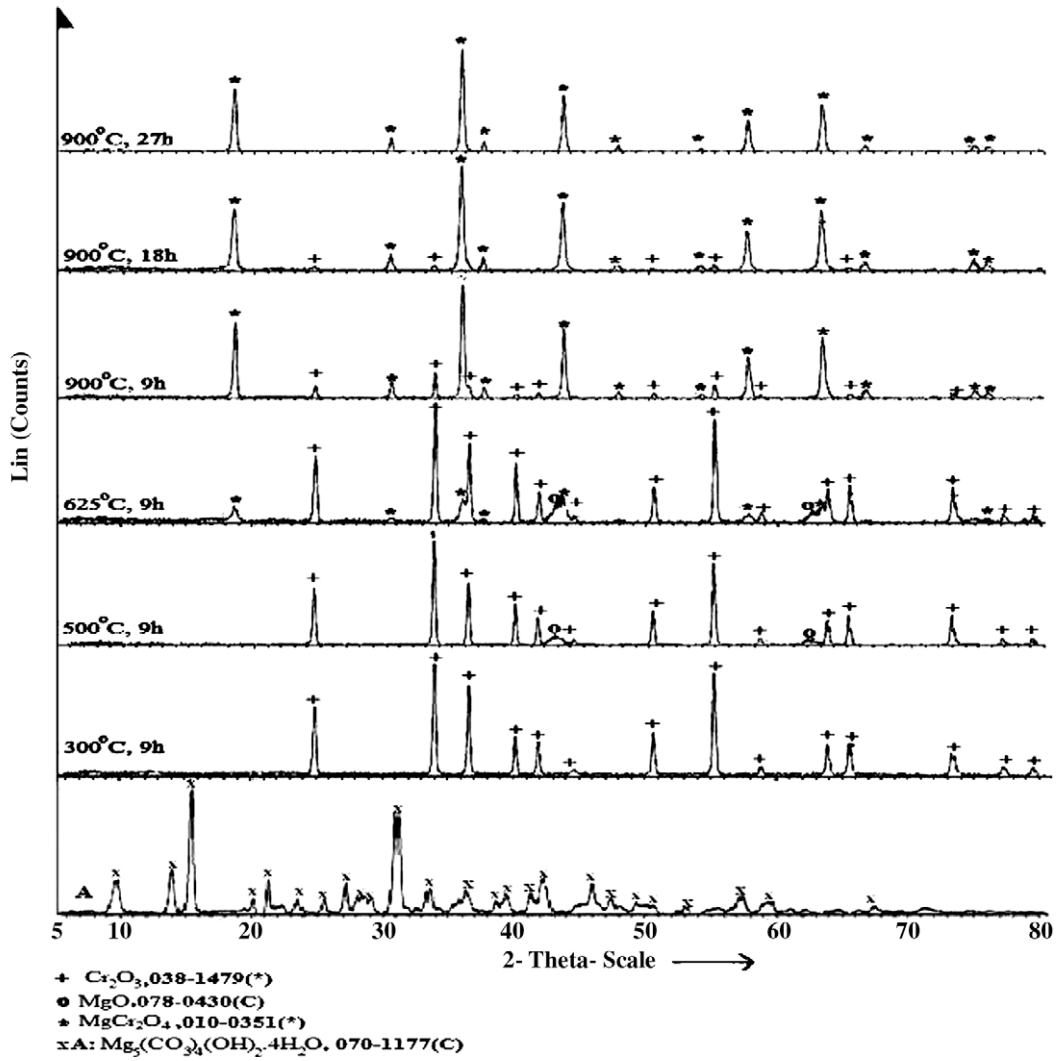

Figure 1 XRPD patterns of un-irradiated ($Mg_5(CO_3)_4(OH)_2{\cdot}4H_2O$) and the calcined un-irradiated mixtures at different temperatures for different time duration.

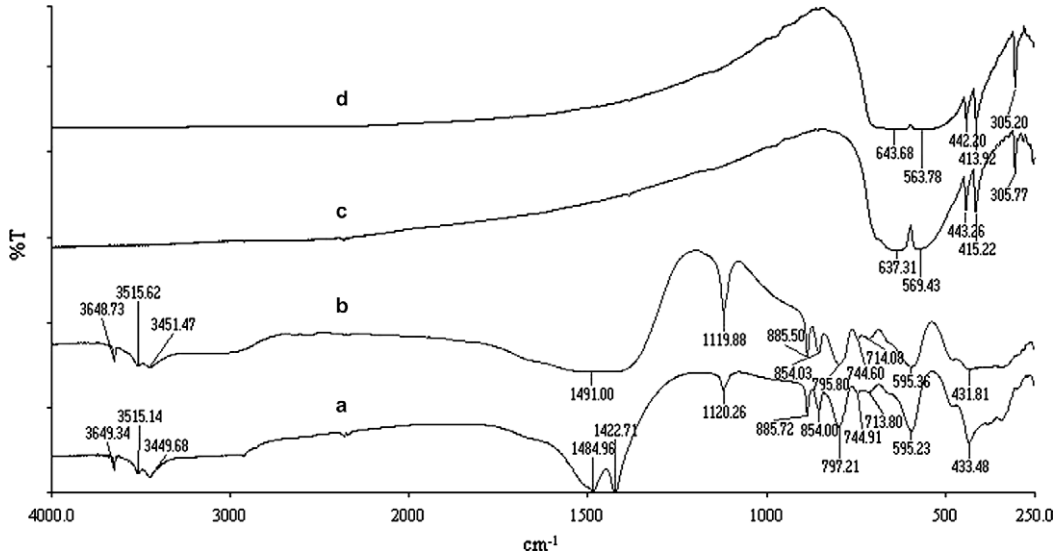

Figure 2 FT-IR spectra of un-irradiated (a and c) and irradiated (b and d) of $Mg_5(CO_3)_2(OH)_2{\cdot}4H_2O$ and Cr_2O_3, respectively.

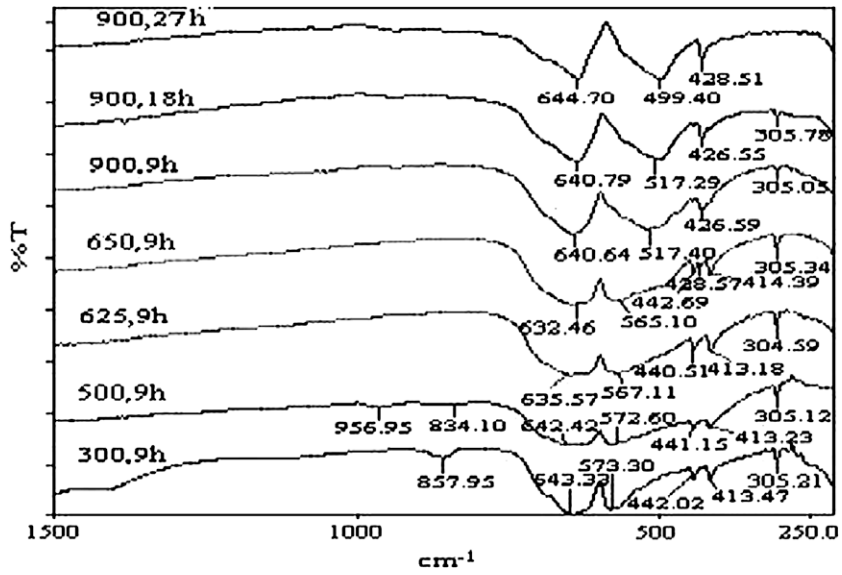

Figure 3 FT-IR spectra of un-irradiated calcined mixtures at different temperatures for different time duration.

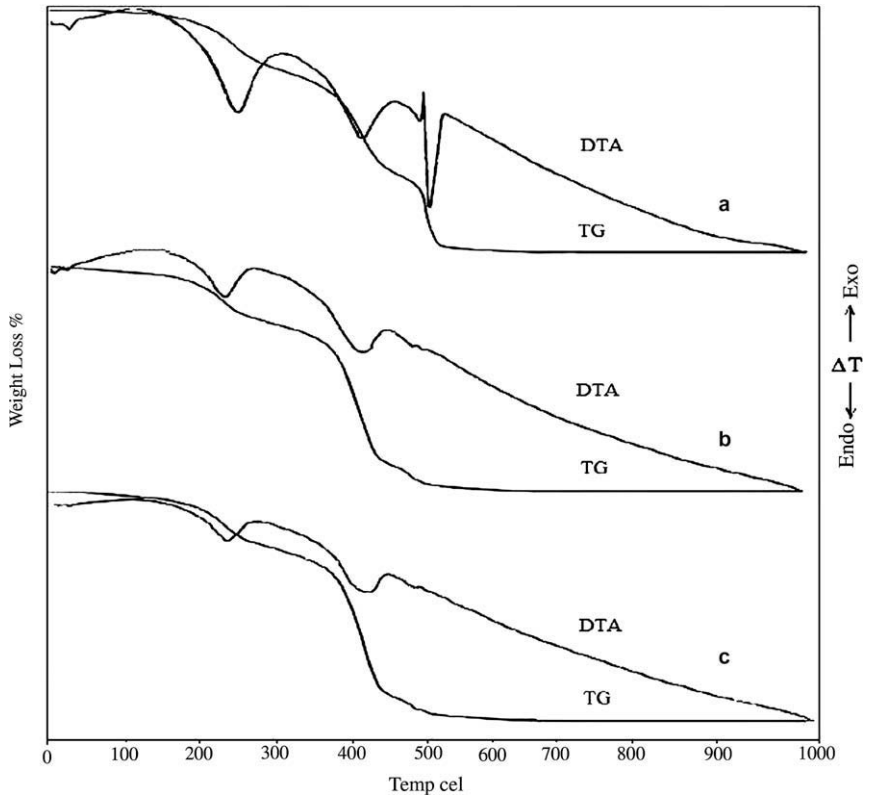

Figure 4 TG/DTA curves of $Mg_5(CO_3)_4(OH)_2{\cdot}4H_2O$ (a), physical crystalline mixtures before (b) and after (c) irradiation.

magnesium chromite. The decomposition behavior of γ-irradiated mixture is similar to that of un-irradiated mixture as we seen in Fig. 1c. Thus, γ-irradiation has no apparent effect on the decomposition behavior of γ-irradiated physical mixture with 10^2 kGy total dose.

Based on the foregoing discussion of XRPD, FT-IR, TG and DTA analysis the following Scheme 1, for decomposition of the investigated crystalline mixture and formation of chromite spinel could be suggested.

4. Kinetic studies

Heterogeneous solid-state reaction can empirically be described by a single-step kinetic equation:

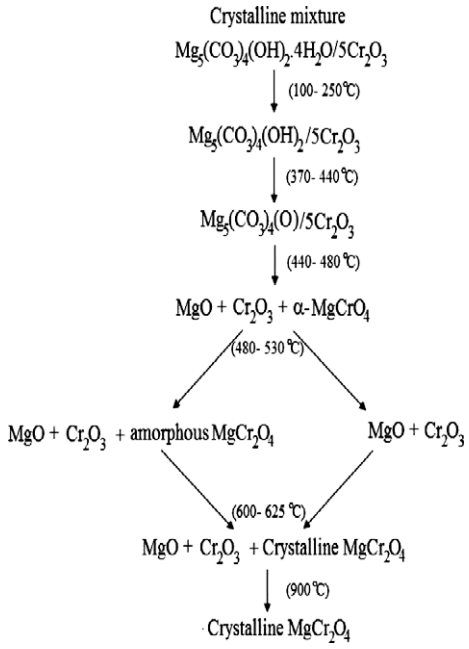

Scheme 1 The proposed reaction mechanism or the thermal decomposition of the investigated crystalline mixture and formation of chromite spinel.

$$\frac{d\alpha}{dt} = k(T)f(\alpha) \tag{1}$$

where t is the time (min^{-1}), T is the temperature (K), k is the reaction rate constant, α is the extent of conversion ($\alpha = \{W_0 - W/W_0 - W_\infty\}$; W_0 is the initial weight of the sample (mg), W is the sample weight (mg) at any temperature T and W_∞ is the final sample weight (mg)), $d\alpha/dt$ is the reaction rate (min^{-1}) and $f(\alpha)$ is the reaction model. The reaction model may take various forms (Sharp et al., 1966; Galway and Brown, 1999), some of which are given in Table 1.

The rate constant, k, usually has an Arrhenius temperature dependence

$$k = A\exp\left(\frac{-E_a}{RT}\right) \tag{2}$$

where A (min^{-1}) is pre-exponential factor, E_a is the activation energy (kJ mol^{-1}) and R is the universal gas constant.

Replacing $k(T)$ in Eq. (1) with the Arrhenius equation gives

$$\frac{d\alpha}{dt} = A\exp\left(\frac{-E_a}{RT}\right)f(\alpha) \tag{3}$$

Under a nonisothermal condition, at constant heating rate $\beta = dT/dt$ Eq. (3) may be written as

$$\frac{d\alpha}{dT} = \frac{d\alpha}{dt}\left(\frac{1}{\beta}\right) = \frac{A}{\beta}\exp\left(\frac{-E_a}{RT}\right)f(\alpha) \tag{4}$$

Upon integration Eq. (4) gives

$$g(\alpha) = \frac{A}{\beta}\int_0^T \exp\left(\frac{-E_a}{RT}\right)dT \tag{5}$$

If E_a/RT is replaced by (x) and integration limits are transformed then Eq. (5) becomes

$$g(\alpha) = \frac{AE_a}{\beta R}\int_x^\infty \frac{e^{-x}}{x^2}dx \tag{6}$$

Eq. (6) can be written as

$$g(\alpha) = \frac{AE_a}{\beta R}P(x) = \frac{A}{\beta}I(Ea, T) \tag{7}$$

The exponential integral ($P(x)$) has no analytical solution but has many approximations (Khawam and Flanagan, 2005).

Kinetic parameters can be obtained from nonisothermal rate laws by both model-fitting and isoconversional (model-free) methods.

Force-fitting experimental data to different model function $f(\alpha)$ is denoted as model-fitting methods, after the $f(\alpha)$ model has been selected from the best linear fit for a series of temperature, $k(T)$ is evaluated (Rodante et al., 2002).

Table 1 Algebraic expressions of $f(\alpha)$ and $g(\alpha)$ for the reaction models considered in the present work.

Symbol	No.	Reaction model	$f(\alpha)$	z
1	D_1	One-dimensional diffusion	$1/2\alpha$	α^2
2	D_2	Two-dimensional diffusion (bi-dimensional particle shape) Valensi equation	$1/[-\ln(1-\alpha)]$	$(1-\alpha)\ln(1-\alpha)+\alpha$
3	D_3	Three-dimensional diffusion (tri-dimensional particle shape) Jander equation	$3(1-\alpha)^{1/3}/2[(1-\alpha)^{-1/3}-1]$	$[1-(1-\alpha)^{1/3}]^2$
4	D_4	Three-dimensional diffusion (tri-dimensional particle shape) Ginstling–Brounshtein	$3/2[(1-\alpha)^{-1/3}-1]$	$(1-2\alpha/3)-(1-\alpha)^{2/3}$
5	R_2	Phase-boundary controlled reaction (contracting area, i.e., bi-dimensional shape)	$2(1-\alpha)^{1/2}$	$[1-(1-\alpha)^{1/2}]$
6	R_3	Phase-boundary controlled reaction (contracting volume, i.e., tri-dimensional shape)	$3(1-\alpha)^{2/3}$	$[1-(1-\alpha)^{1/3}]$
7	F_1	First-order (Mampel)	$(1-\alpha)$	$[-\ln(1-\alpha)]$
8	F_2	Second-order	$(1-\alpha)^2$	$(1-\alpha)^{-1}-1$
9	F_3	Third-order	$(1-\alpha)^3$	$(1/2)[(1-\alpha)^{-2}-1]$
10	$F_{3/2}$	Three-halves order	$(1-\alpha)^{3/2}$	$2[(1-\alpha)^{-1/2}-1]$
11	A_2	Avrami-Erofeev ($n = 2$)	$2(1-\alpha)[-\ln(1-\alpha)]^{1/2}$	$[-\ln(1-\alpha)]^{1/2}$
12	A_3	Avrami-Erofeev ($n = 3$)	$3(1-\alpha)[-\ln(1-\alpha)]^{2/3}$	$[-\ln(1-\alpha)]^{1/3}$
13	$A_{3/2}$	Avrami-Erofeev ($n = 1.5$)	$(3/2)(1-\alpha)[-\ln(1-\alpha)]^{1/3}$	$[-\ln(1-\alpha)]^{2/3}$
14	A_4	Avrami-Erofeev ($n = 4$)	$4(1-\alpha)[-\ln(1-\alpha)]^{3/4}$	$[-\ln(1-\alpha)]^{1/4}$

Model-free isoconversional methods allow for estimating the activation energy as function of α without choosing the reaction model, the basic assumption of these methods is that the reaction rate of constant extent of conversion α depends only on the temperature. Hence, constant E_a value can be expected in the case of single stage decomposition, while for multi-step process E_a varies with α due to the variation in the relative contributions of single steps to the overall reaction rate (Khawam and Flanagan, 2005; Vyazovkin and Sbirrazzuoli, 2002).

5. Model-fitting approach

There are several nonisothermal model-fitting methods. One of the most popular is the Coats and Redfern method (CR method), which utilizes the asymptotic series expansion in approximating $P(x)$ Eq. (7), producing the following equation:

$$\ln\frac{g(\alpha)}{T^2} = \ln\left(\frac{AR}{\beta E_a}\left[1-\left(\frac{2RT^*}{\beta E_a}\right)\right]\right) - \frac{E_a}{RT} \tag{8}$$

where T^* is the mean experimental temperature.

The other method proposed by Clark and Kennedy (CK method) is based on the expression, $T = \beta t + T^0$, where T^0 is initial temperature.

The basic equation is:

$$\frac{\beta g(\alpha)}{T-T^0} = A\exp\left(-\frac{E_a}{RT}\right) \tag{9}$$

Taking the logarithm of both sides of the equation:

$$\ln\frac{\beta g(\alpha)}{T-T^0} = \ln A - \frac{E_a}{RT} \tag{10}$$

Plotting the left-hand side of both Eqs. (8) and (10) against $1/T$ should give straight lines for the reaction models listed in Table 1 (Vyazovkin and Wight, 1999) and the result are shown in Fig. 5. From the slope and intercept we can determine E_a and $\ln A$, respectively.

The values of activation energy (E_a), pre-exponential factors (lnA) and the coefficients of linear correlations (r) for kinetic models are presented in Table 2. The correlation coefficient (r) is sometimes used as a parameter for choosing the best model.

As listed in Table 2 for both applied methods (CR and CK methods), it can be found that D_1 is the best model show the linear relationships of the data for both irradiated and un-irradiated mixtures. The values of E_a, $\ln A$ (Arrhenius parameters) and r obtained from CR and CK methods using the selected model for the processes obtained in Table 2 are very low. From this fact it may be concluded that the reaction under consideration is a typical complex multi-step reaction with more than one mechanism.

5.1. Model-free approach

The Kissinger–Akahira–Sunose method (KAS method) is based on the Coats–Redfern approximation of $P(x) \cong (\exp(-x))/x^2$ which transformed Eq. (7) to:

$$\ln\left(\frac{\beta}{T^2}\right) = \ln\frac{AR}{E_a g(\alpha)} - \frac{E_a}{RT} \tag{11}$$

Another method proposed by Tang (T method) is based on the approximate formula which introduced into Eq. (7). Taking the logarithms of both sides, Eq. (12) is obtained as:

$$\ln\left(\frac{\beta}{T^{1.894661}}\right) = \ln\left[\frac{AE_a}{Rg(\alpha)}\right] + 3.635041 - 1.894661\ln E_a - 1.001450\frac{E_a}{RT} \tag{12}$$

A plot of the left-hand sides of both Eqs. (11) and (12) versus $1/T$ give a group of straight lines at each α (Vyazovkin and Wight, 1999) as can be seen in Fig. 6, which give apparent activation energy from the slope for a particular α without considering a selected model.

The Vyazovkin isoconversional method (VYZ method) (Vyazovkin and Wight, 1999; Janković et al., 2007) is a nonisothermal method which utilizes an accurate nonlinear Senium-Yang approximation of $P(x)$ (Eq. (7)), which leads to:

$$\Omega = \left|\sum_{i=1}^{n}\sum_{i\neq j}^{n}\frac{I(E_{a,\alpha},T_{\alpha,i})\beta_j}{I(E_{a,\alpha},T_{\alpha,j})\beta_i}\right| \tag{13}$$

$$I(Ea,\alpha,T\alpha) = \int_0^{T_{\alpha i}}\exp\left(\frac{-E_{a,\alpha}}{RT}\right)dT \tag{14}$$

where n the number of heating rates, $I(E_{a,\alpha}, T_\alpha)$ the exponential integral ($P(x)$) that results from heating rate β. The 5th degree Senum-Yang approximation was chosen for our work.

The $E_{a,\alpha}$ can be determined at any particular value of α by finding the value of E_α for which the objective function Ω is minimized.

The temperature integral can be evaluated by several approximation. We have used Gorbachev, Agrawal and

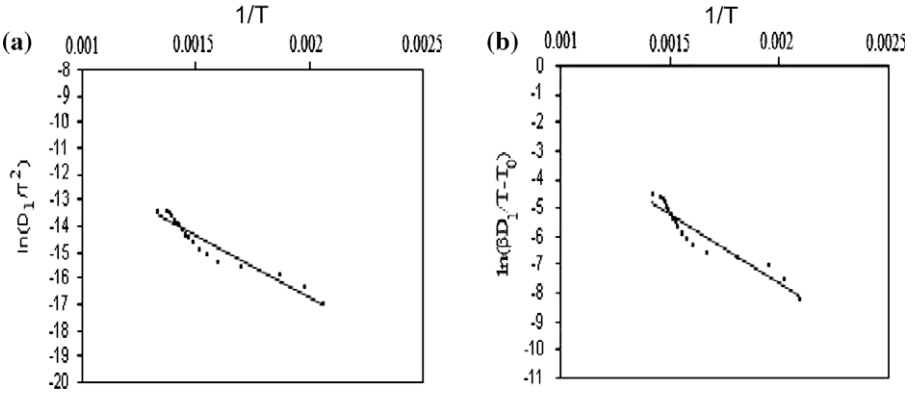

Figure 5 (a) CR method and (b) CK method.

Table 2 Kinetic parameter determind by CR and CK methods.

Model	CR						CK					
	E		$\ln A$		r		E		$\ln A$		r	
	Un-irradiated	Irradiated	Un-irradiated	Irradiated	Un-irradiated	Irradiated	Un-irradiated	Irradiated	Un-irradiated	Irradiated	Un-irradiated	Irradiated
D_1	39.2464	40.03058	4.22043	4.314446	91.528	92.324	39.05335	39.99566	2.50784	2.61826	91	91.982
D_2	44.26224	45.23348	4.800317	4.925812	89.362	90.384	44.06919	45.13837	3.00946	3.13678	88.806	89.9
D_3	50.69728	51.84427	4.901847	5.052753	86.026	87.194	50.50439	51.749	3.01522	3.16666	85.46	86.696
D_4	46.70489	47.40077	3.828872	3.957691	88.27	89.344	46.17945	47.30533	2.001	2.13616	87.704	88.85
R_3	18.84302	20.95361	0.471686	0.481407	82.33	82.284	18.65013	20.8585	−1.03556	−0.99312	80.712	80.93
R_2	20.4275	19.29513	0.419865	0.522472	80.626	83.788	20.23461	19.23261	−1.06906	−0.96554	79.074	82.552
A_2	7.04249	–	–	–	55.174	58.306	6.849522	7.212328	−2.1533	−2.10832	50.74	54.498
A_3	1.414162	–	–	–	10.664	13.266	1.221194	1.464228	−3.15334	−3.12316	6.954	10.17
$A_{3/2}$	12.67087	-	1.043867	–	68.484	70.568	7.482101	12.96053	−1.1533	−1.09346	65.778	68.458
A_4	–	–	–	–	18.854	17.928	–	–	−3.72528	−3.63062	18.498	15.686
F_1	23.92719	24.55174	2.342056	2.438306	76.942	78.648	23.73431	24.45679	0.84674	0.9363	75.544	77.418
F_2	37.05384	38.06748	4.591417	5.691372	66.106	67.818	36.86095	37.97237	3.87932	4.02374	65.174	67.002
F_3	53.49527	54.83765	7.313669	9.754276	58.818	60.462	53.13594	54.74254	7.6117	7.8265	58.198	59.924
$F_{3/2}$	30.01919	30.82133	7.016659	3.937283	71.25	72.98	29.82598	30.72638	2.2576	2.37312	70.098	71.964
P_1	–	–	–	–	89.794	90.326	–	–	−4.19572	−4.18152	86.678	86.986
P_2	–	–	–	–	47.984	48.426	–	–	−3.8765	−3.86118	45.342	43.424
P_3	2.620722	–	–	–	45.912	48.986	2.236749	2.474895	−3.23806	−3.21012	34.73	41.668
P_4	26.97411	27.58386	2.119116	2.195114	90.048	91.302	26.78106	27.48874	0.59254	0.67548	89.428	90.606

Sivasubramanian and Cai for integration of Eq. (14) (Ghoshal and Saha, 2006; Maiti et al., 2006).

$$\int_0^T \exp\left(\frac{-E_\alpha}{RT_{\alpha i}}\right)dT = \frac{RT_{\alpha i}^2}{E_\alpha}\left(\frac{1}{1+\frac{2RT}{E\alpha}}\right)\exp\left(\frac{-E\alpha}{RT}\right) \tag{15}$$

$$\int_0^T \exp\left(\frac{-E_\alpha}{RT_{\alpha i}}\right)dT = \frac{RT_{\alpha i}^2}{E_\alpha}\left[\frac{1-2RT/E_\alpha}{1-5(ER/E_\alpha)^2}\right]\exp\left(\frac{-E_\alpha}{RT_{\alpha i}}\right) \tag{16}$$

$$\int_0^T \exp\left(\frac{-E_\alpha}{RT_{\alpha i}}\right)dT = \frac{RT_{\alpha i}^2}{E_\alpha}\left[\frac{E_\alpha/RT_{\alpha i}+0.66691}{E_\alpha/RT_{\alpha i}+2.64943}\right]\exp\left(\frac{-E_\alpha}{RT_{\alpha i}}\right) \tag{17}$$

Fig. 7 shows the variation of apparent activation energy $E_{a,\alpha}$, as a function of the extent of conversion α of the data for un-irradiated and γ-irradiated mixtures. From Fig. 7 we can recognized that the dependence of $E_{a,\alpha}$ on α is almost the same by using different isoconversional methods. And these differences in the values of $E_{a,\alpha}$ could be due to the approximation of temperature integral that were used in the derivations of relations that ground KAS, T and VYZ methods (Vyzovkin and Wight, 1999). Also, Fig. 7 shows that, the values of $E_{a,\alpha}$ for γ-irradiated mixture are reduced compared to un-irradiated one. The reducing of the values of activation energy of the decomposition reaction could be attributed to the formation of additional nucleation sites and reactive centers. From the dependence of $E_{a,\alpha}$ on α we can assumed that there are at least two steps, the first step at $\alpha < 0.3$ show decrease of activation energy by increase extant of conversion which is lie to dehydration process, the second step at $\alpha > 0.3$ which is show an increase of the activation energy by increase extent of conversion which lie to decarbonation and formation of the magnesium chromite.

5.2. Compensation effect

Use of the artificial isokinetic relationship (IKR) that occurs on fitting various reaction models to the same set of nonisothermal kinetic data can be used to evaluate $\ln A$.

$$\ln A_j = a + bE_{a,j} \tag{18}$$

where j refers to one of the possible models $f_j(\alpha)$ assumed to describe the process. The parameters of Eq. (18) are $a = \ln k_{\text{iso}}$ and $b = 1/RT_{\text{iso}}$ (Agrwal, 1986). Fig. 8 shows the artificial isokinetic relationship for the process obtained by CK method. The values of a, b, k_{iso}, T_{iso} of Eq. (18) obtained by (CK) model-fitting are given in Table 3.

It can be seen that the isokinetic temperatures (T_{iso}) lying in the region of the experimental temperature and this indicates that the reaction model $f(\alpha)$ was properly chosen.

Once the correlation parameters a and b have been evaluated, the $E_{a,\alpha}$ values are substituted for $E_{a,j}$ in Eq. (18) to estimate the corresponding $\ln A_\alpha$ values and obtaining the dependence of $\ln A_\alpha$ on α for multi-step processes (Vyzovkin and Wight, 1999).

Fig. 9 shows the variation of the $\ln A_\alpha$ as a function of extent of conversion α, which was obtained by different isoconversional methods for the process.

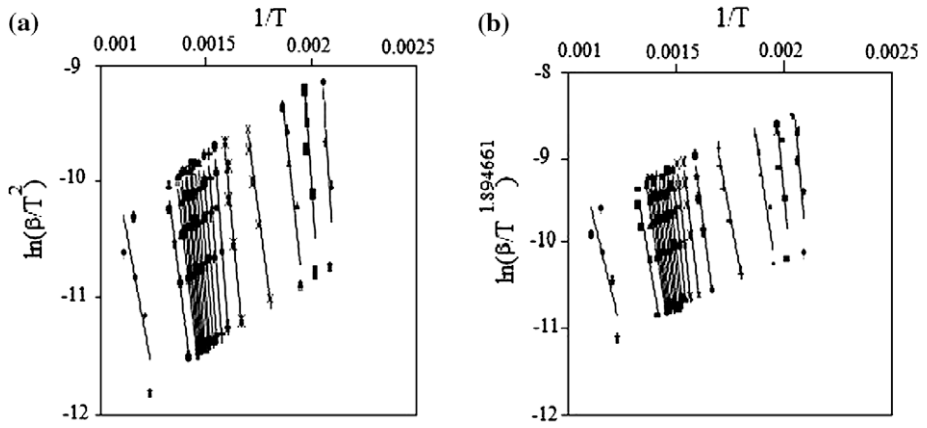

Figure 6 (a) KAS method and (b) T method.

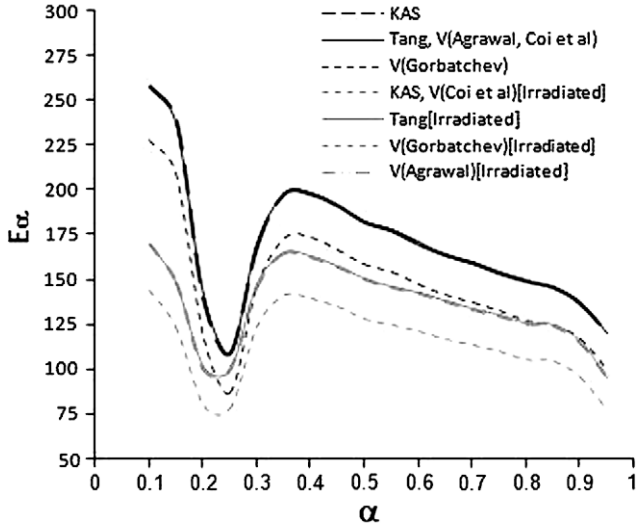

Figure 7 The activation energy plotted as a function of the extent of the conversion.

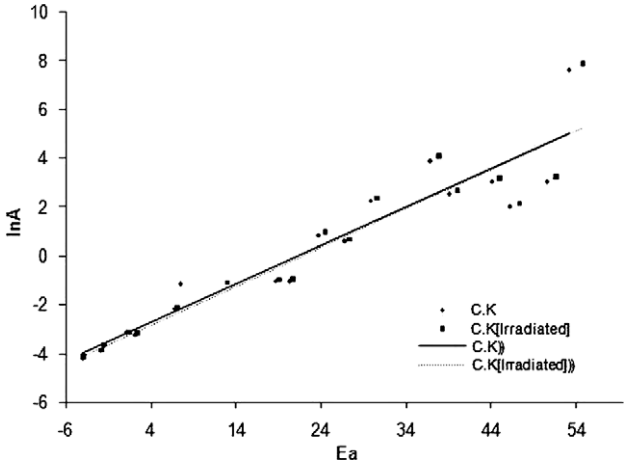

Figure 8 The isokinetic relationships obtain by CK method.

Table 3 Artificial isokinetic parameter obtained by CK method.

Method	a (min^{-1})	b (mol kJ^{-1})	k_{iso} (min^{-1})	T_{iso} (K)	r
KC	−3.396	0.158	0.0335	759.82	0.896
KC (irradiation)	−3.488	0.159	0.0306	753.63	0.905

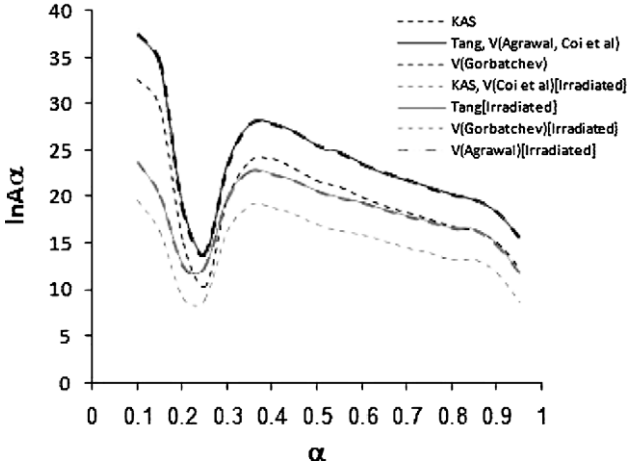

Figure 9 Dependence of the $\ln A_\alpha$ on extent of conversion, estimated from Eq. (18) for the different isoconversional methods.

It can be seen that the $\ln A_\alpha$ shows the same dependence on α as the apparent activation energy $E_{a,\alpha}$ in Fig. 7. This behavior supported the conclusion mentioned above.

5.3. Simulation

Simulated data are the only data for which Arrhenius parameters and reaction models are known exactly (Vyazovkin, 2000). The data were simulated according to the scheme of two reaction mechanisms

$$\left.\begin{aligned} A_{(s)} &\rightarrow B_{(s)} + C_{(g)} \\ B_{(s)} &\rightarrow D_{(s)} + E_{(g)} \end{aligned}\right\} \quad (19)$$

The overall reaction rate of these processes is:

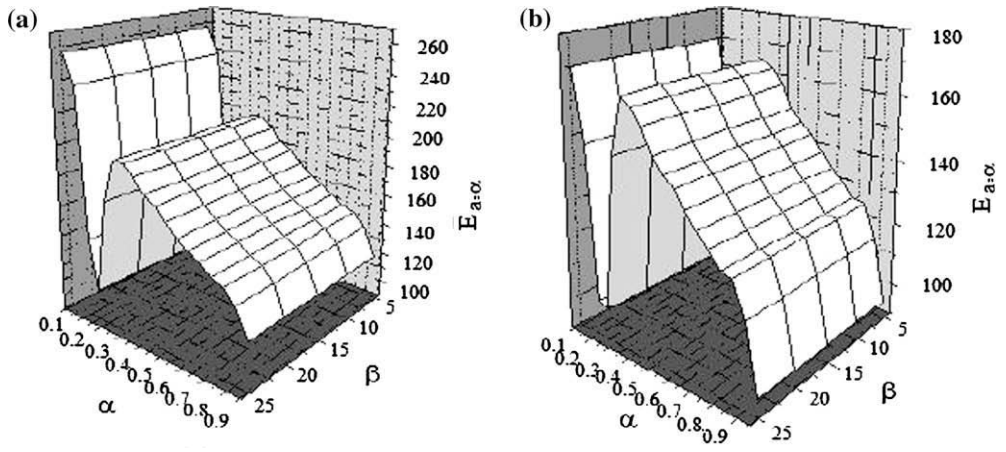

Figure 10 Surface plot of activation energy for simulated process before irradiation (a) and after irradiation.

$$\frac{d\alpha}{dt} = \frac{1}{2}\left(\frac{d\alpha_1}{dt} + \frac{d\alpha_2}{dt}\right) = \frac{1}{2}[k_1(T)f(\alpha_1) + k_2(T)f(\alpha_2)] \tag{20}$$

The Arrhenius parameters of the individual steps were taken so that $A_1 = 10^{31}\ \mathrm{min}^{-1}$, $E_1 = 260\ \mathrm{kJ\ mol}^{-1}$, $A_2 = 10^{10}\ \mathrm{min}^{-1}$ and $E_2 = 80\ \mathrm{kJ\ mol}^{-1}$. The values were chosen to make rates of two steps are comparable within the working range temperature.

Integration of Eq. (20) for nonisothermal condition has give rise to reaction dependence of α versus T.

By assumption that, the processes contain at least two steps with different reaction mechanism. The first mechanism is third-order reaction (F_3) model, and the second mechanism is diffusion in one-dimensional (D_1) model. Then the effective activation energy of the overall process can be written as:

$$E_{a,\alpha} = -R\left[\frac{d\ln(d\alpha/dt)}{dT^{-1}}\right]_\alpha = \frac{E_1k_1(T)f(\alpha_1) + E_2k_2(T)f(\alpha_2)}{k_1(T)f(\alpha_1) + k_2(T)f(\alpha_2)}$$
$$= \frac{E_1k_1(T)f(1-\alpha_1)^3 + E_2k_2(T)f\left(\frac{1}{2}\alpha_2\right)}{k_1(T)f(1-\alpha_1)^3 + k_2(T)f\left(\frac{1}{2}\alpha_2\right)} \tag{21}$$

This is clearly a function of both temperature an extent of conversion. Substitution of depends of a α versus T for various β into Eq. (21) allows surface plots of the effective activation energy as function of α and β to be obtained (Sbirrazzuoli et al., 2000). These plots are shown in Fig. 10.

Acknowledgements

This work was supported by the King Abdullaziz City of Science and Technology in Saudi Arabia. Also the authors thanks Dr. Ahmed Basfar for his supported and advice.

References

Agrwal, R.K., 1986. On the compensation effect. Journal of Thermal Analysis 31, 73–86.

Al-Farhan, K.A., 1999. A qualitative and quantitative PC program for X-ray powder diffraction. Powder Diffraction 14 (1), 16–21.

Bhatta, D., Nayak, H., 2002. Catalytic effects of magnesium chromite spinel on the decomposition of lanthanum oxalate. Thermochimica Acta 389, 109–119.

Criado, J., Gonzalez, F., Morales, J., 1979. Alteration of kinetics and thermodynamics of thermal decomposition of Alkaline-Earth carbonates induced by grinding. Thermochimica Acta 32, 99–110.

Docherty, F.T., Craven, A.J., McComb, D.W., Skakle, J., 2001. ELNES investigations of the oxygen K-edge in spinels. Ultramicroscopy 86, 273–288.

Galway, A.K., Brown, M.E., 1999. Thermal Decomposition of Ionic Solids. Elsevier Science B.V.

Gengembre, L., Sloczynski, J., Ziolkowski, J., Grzybowska, B., Grabowski, R., Jachewicz, D., Wcislo, K., 1999. Oxidative dehydrogenation of propane on $Ni_xMg_{1-x}Al_2O_4$ and $NiCr_2O_4$ spinels. Journal of Catalysis 187, 410–418.

Ghoshal, A.K., Saha, B., 2006. Model-free kinetics analysis of waste PE sample. Thermochimica Acta 451, 27–33.

Hartman, M., Trnka, O., Svoboda, K., 1994. Decomposition kinetics of Alkaline-Earth hydroxides and surface-area of their calcines. Chemical Engineering Science 49, 1209–1216.

Janković, B., Adnadević, B., Jovanović, J., 2007. Application of model-fitting and model-free kinetics to the study of non-isothermal dehydration of equilibrium swollen poly (acrylic acid) hydrogel: thermogravimetric analysis. Thermochimica Acta 452 (2), 106–115.

Khan, N., Dollimore, D., Alexander, K., Wilburn, F., 2001. The origin of the exothermic peak in the thermal decomposition of basic magnesium carbonate. Thermochimica Acta 367, 321–333.

Khawam, A., Flanagan, D.R., 2005. Role of isoconversional methods in varying activation energies of solid-state kinetics II. Nonisothermal kinetic studies. Thermochimica Acta 436, 101–112.

Mahfouz, R.M., Monshi, M.A.S., Alshehri, S.M., Abd El-Salam, N.M., 2000. Isothermal decomposition of γ-irradiated samarium acetate. Radiation Physics and Chemistry 59, 381–385.

Mahfouz, R.M., Monshi, M.A.S., Alshehri, S.M., Abd El-Salam, N.M., 2000. Kinetics of the thermal decomposition of γ-irradiated cobaltous acetate. Thermochimica Acta 363, 61–70.

Maiti, A.K., Ghoshal, A.K., Saha, B., 2006. Model-free method for isothermal and non-isothermal decomposition kinetics analysis of PET sample. Thermochimica Acta 444, 46–52.

Monshi, M.A.S., Abd El-Salam, N.M., Mahfouz, R.M., 1998. Isothermal decomposition of γ-irradiated uranyl acetate. Thermochimica Acta 322, 33–37.

Rodante, F., Vecchio, S., Tomassetti, M., 2002. Kinetic analysis of thermal decomposition for penicillin sodium salts – model-fitting and model-free methods. Journal of Pharmaceutical and Biomedical Analysis 29, 1031–1043.

Roy, R., White, W.B., Muller, O., 1969. Infrared spectra of the chromates of magnesium, nickel and cadmium. Spectrochimica Acta 25, 1491–1499.

Sawada, Y., Yamaguchi, J., Sakurai, O., Uematsu, K., Mizutani, N., Kato, M., 1979a. Thermal decomposition of basic Magnesium

Carbonates under high-pressure gas atmospheres. Thermochimic Acta 32, 277–291.

Sawada, Y., Yamaguchi, J., Sakurai, O., Uematsu, K., Mizutani, N., Kato, M., 1979b. Thermogravimetric study on the decomposition of hydromagnesite $4Mg(CO_3)\cdot Mg(OH)_2\cdot 4H_2O$. Thermochimica Acta 33, 127–140.

Sawada, Y., Yamaguchi, J., Sakurai, O., Uematsu, K., Mizutani, N., Kato, M., 1979c. Isothermal differential calorimetry on an exothermic phenomenon during thermal decomposition of hydromagnesite $4Mg(CO_3)\cdot Mg(OH)_2\cdot 4H_2O$. Thermochimica Acta 34, 233–237.

Sbirrazzuoli, N., Vyazovkin, S., Vincent, L., 2000. Comparison of several computational procedures for evaluating the kinetics of thermally stimulated condensed phase reactions. Chemometrics and Intelligent Laboratory Systems 54, 53–60.

Sharp, J., Brindley, G., Achar, B., 1966. Numerical data for some commonly used solid state reaction equations. Journal of American Ceramic Society 49 (7), 379–382.

Shimizu, Y., Kusano, S., Kuwayama, H., Tanaka, K., Egashira, M.J., 1990. Oxygen-sensing properties of spinel-type oxides for stoichiometric air/fuel combustion control. American Ceramic Society 73, 818–824.

Spinks, J.W.T., Woods, R.J., 1990. An Introduction to Radiation Chemistry. Wiley, New York.

Vyzovkin, S., Wight, C., 1999. Model-free and model-fitting approaches to kinetic analysis of isothermal and nonisothermal data. Thermochimica Acta 340–341, 53–68.

Vyazovkin, S., 2000. Computational aspects of kinetic analysis. Part C. The ICTAC Kinetics Project – the light at the end of the tunnel. Thermochimica Acta 355, 55–163.

Vyazovkin, S., Sbirrazzuoli, N., 2002. Learning about epoxy cure mechanisms from isoconversional analysis of DSC data. Thermochimica Acta 388, 289–298.

White, W., 1971. Infrared characterization of water and hydroxyl ion in the basic magnesium carbonate minerals. The American Mineralogist 56, 46–53.

Williey, R.J., Noirclerc, P., Busca, G., 1993. Preparation and characterization of magnesium chromite and magnesium ferrite aerogels. Chemical Engineering Communication 123, 1–16.

التحليل الحركي للانحلال عند تغير درجات الحرارة للخليط البلوري $(Mg_5(CO_3)_4(OH)_2.4H_2O/5Cr_2O_3)$

أسماء بنت عبدالله العثمان، خالد بن عبدالرحمن الفرحان، رفعت محمد محفوظ

قسم الكيمياء، كلية العلوم، جامعة الملك سعود، الرياض

المملكة العربية السعودية

البريد الإلكتروني: asmaalothman@yahoo.com

هاتف 00966507292527 ; فاكس 0096614874595

(قدم للنشر في 1429/1/25هـ؛ وقبل للنشر في 1429/4/13هـ)

الكلمات المفتاحية: التحلل الحراري، النموذج المقيد، النموذج الحر، ثبوت الحركية، الدوال الحركية، سبينل$MgCr_2O_4$.

ملخص البحث. تم تحضير سبينل نقي من رفع درجة حرارة الخليط البلوري $(Mg_5(CO_3)_4(OH)_2.4H_2O/ 5Cr_2O_3)$ عند 900 °C لمدة 27 ساعة. استخدمت تقنيات TG و DTA و FTIR وXRPD لتتبع التفاعل والتعرف على النواتج. تم دراسة حركية الانحلال الحراري عند تغير درجات الحرارة للخليط البلوري الفيزيائي غير المشعع والمشعع في الهواء الثابت, وتقدير الدوال الحركية من خلال تقريبات النماذج المقيدة والحرة وعلاقة ثبوت الحركية للعمليات عديدة الخطوات (IKR). أظهرت النتائج أن انحلال الخليطين (غير المشعع والمشعع) يتم بخطوتين متتابعتين بميكانيكيتين مختلفتين, الأولى ميكانيكية التفاعل من الرتبة الثالثة (F_3), والثانية ميكانيكية الانتشار في بعد واحد (D_1).